Phys. Status Solidi B **251**, No. 1, 81–96 (2014) / **DOI** 10.1002/pssb.201350156

physica status solidi b
www.pss-b.com
basic solid state physics

Part of Topical Section on Computational Thermodynamics

Feature Article

Including the effects of pressure and stress in thermodynamic functions

T. Hammerschmidt*[,1], I. A. Abrikosov[2], D. Alfè[3], S. G. Fries[1], L. Höglund[4], M. H. G. Jacobs[5], J. Koßmann[1], X.-G. Lu[6], and G. Paul[7]

[1] ICAMS, Ruhr-Universität Bochum, Bochum, Germany
[2] Department of Physics, Chemistry and Biology (IFM), Linköping University, Linköping, Sweden
[3] Department of Earth Sciences, London Centre for Nanotechnology, Department of Physics and Astronomy and Thomas Young Centre@UCL, University College London, WC1E 6BT, United Kingdom
[4] KTH Royal Institute of Technology, Department of Materials Science and Engineering, Stockholm, Sweden
[5] Institute of Metallurgy, Clausthal University of Technology, Clausthal-Zellerfeld, Germany
[6] School of Materials Science and Engineering, Shanghai University, Shanghai, P. R. China
[7] ThyssenKrupp Steel Europe, Duisburg, Germany

Received 28 August 2013, revised 8 November 2013, accepted 12 November 2013
Published online 19 December 2013

Keywords CALPHAD, DFT calculations, elastic constants, pressure, strain

* Corresponding author: e-mail thomas.hammerschmidt@rub.de, Phone: +49 234 3229375, Fax: +49 234 3214977

Most applications of thermodynamic databases to materials design are limited to ambient pressure. The consideration of elastic contributions to thermodynamic stability is highly desirable but not straight-forward to realise. We present examples of existing physical models for pressure-dependent thermodynamic functions and discuss the requirements for future implementations given the existing results of experiments and first-principles calculations. We briefly summarize the calculation of elastic constants and point out examples of nonlinear variation with pressure, temperature and chemical composition that would need to be accounted for in thermodynamic databases. This is particularly the case if a system melts from different phases at different pressures. Similar relations exist between pressure and magnetism and hence set the need to also include magnetic effects in thermodynamic databases for finite pressure. We present examples to illustrate that the effect of magnetism on stability is strongly coupled to pressure, temperature, and external fields. As a further complication we discuss dynamical instabilities that may appear at finite pressure. While imaginary phonon frequencies may render a structure unstable and destroy a crystal lattice, the anharmonic effects may stabilize it again at finite temperature. Finally, we also outline a possible implementation scheme for strain effects in thermodynamic databases.

1 Introduction

1.1 Motivation The CALPHAD method [1] is an established technique in alloy design. Commercial software packages like Thermo-Calc [2] and FactSage [3] are applied to calculate phase diagrams and to determine precipitation and dissolution temperatures [4, 5]. Further the Gibbs energy and its derivatives are essential data for kinetic models. Alloy design is usually focused on target properties like mechanical properties, formability, toughness, corrosion resistance, coating and welding properties. As most of these properties are linked to the non-equilibrium microstructure and chemical composition this connection is often established by experience. The mechanical properties of materials are essential for designing mechanical structures like, e.g. bridges, planes, cars, and even buildings that have to resist the static and dynamic forces considered for ordinary usage within their elastic range. Improved mechanical properties help to optimize the material usage of such technical structures and result in, e.g. lighter vehicles using less fuel and safer constructions using less material. Thus, from an engineering perspective, the knowledge of the mechanical properties and their variation with alloying and temperature are a crucial additional information for materials design, which could be provided within thermodynamic databases. Especially, nonlinear variations would be important for optimization, be it to improve the elastic properties, or to avoid the pitfall

of their sudden drop. But, even on a microstructure scale the elastic properties are an important information, as phase transformations and precipitation processes usually cause local stresses.

1.2 Perspective Most applications of present day thermodynamic databases for metallic systems using the CALPHAD method are limited to ambient pressure, and it is not a trivial task to derive volume properties from them. In geophysical applications, databases of mineral systems developed by, e.g. Fei et al. [6], Saxena [7], Holland and Powell [8] and Fabrichnaya et al. [9] are based on the classical CALPHAD approach extended such that the pressure variable is included in the expression for the Gibbs energy. However, it has been demonstrated in the literature that thermodynamic properties calculated with this approach often show physically unrealistic behaviour in specific regions of the pressure–temperature space. For instance Lu et al. [10] showed that heat capacity at high pressure may become negative for MgO and iron. Guillermet [11] showed that this is also the case for the element molybdenum. Jacobs and Oonk [12] and Jacobs et al. [13] showed that this approach yields erroneously negative thermal expansivities for MgO and $MgSiO_3$ (perovskite). To remedy these difficulties in CALPHAD models, a formalism is required with comparable computational efficiency. Successful attempts have been made by Stixrude and Lithgow-Bertelloni [14], Piazonni et al. [15] and Jacobs and de Jong [16, 17] to develop thermodynamic databases for mineral systems based on lattice vibrational methods, meeting this requirement. These methods allow the calculation of thermodynamic properties free from physically unrealistic behaviour and include also the calculation of the shear modulus in a self-consistent way. Therefore, these methods are especially useful in mineral physics to derive accurate phase diagrams and thermophysical properties in the complete pressure–temperature regime of planetary interiors. Additionally, they are successful in the representation of experimental Hugoniot data (cf. Section 2.2) at extreme conditions, indispensable for developing an accurate pressure scale. Because also experimental data at ambient pressure are represented with high precision it is anticipated that these methods are generally suitable to develop databases in materials sciences, not only for silicate and oxide materials, but also for metallic substances.

2 Physical models for pressure thermodynamic functions

2.1 Debye–Grüneisen model A Helmholtz energy approach, based on the Debye–Grüneisen model, was proposed by Lu et al. [18, 19] to study thermodynamic and thermophysical properties in a wide temperature and pressure range from 0 K upwards and from atmospheric pressure to extremely high pressures. For a non-magnetic system, the total Helmholtz energy is described by summing up three parts: the static lattice energy at 0 K, the lattice vibrational energy and the energy due to the electronic thermal excitations. The lattice vibrational energy is considered based on the quasi-harmonic approximation and the Debye model for which the Debye temperature is determined by an equation of state (EoS) at a reference temperature (0 K or room temperature) and the Grüneisen model. This method can avoid abnormal behavior, e.g. negative entropy and heat capacity observed in the present CALPHAD modelling and can bring physical meaning to several parameters representing both thermodynamic properties, e.g. heat capacity and Gibbs energy, and thermophysical properties, e.g. volume, thermal expansion, bulk modulus and Poisson ratio. An optimum set of parameters is obtained to accurately reproduce most of the experimental data for fcc Cu. The calculated properties at 298.15 K and 101 325 Pa for fcc Cu are listed in Table 1. Ongoing developments include the proper treatment of magnetic properties, e.g. for Fe, Ni and Co, as well as the extension to multi-component systems. Applications and limitations of the Debye model are discussed by Palumbo et al. [27].

Table 1 Calculated [19] and selected experimental values for thermodynamic and thermophysical properties for fcc Cu at 298.15 K and 101 325 Pa. The values for adiabatic Young's modulus, Poisson's ratio, bulk sound velocity and Grüneisen parameter were calculated as average values from data for adiabatic bulk modulus, shear modulus and volume.

isobaric heat capacity ($J\,mol^{-1}\,K^{-1}$)	24.46	24.47 [20]
molar volume ($10^{-6}\,m^3$/mol)	7.1103	7.1109 [21] 7.1100 [22]
lattice parameter (nm)	0.36146	0.36147 [21] 0.36146 [22]
linear thermal expansion ($10^{-5}\,K^{-1}$)	1.652	1.65 [20]
cubic thermal expansion ($10^{-5}\,K^{-1}$)	4.956	4.95 [20]
adiabatic bulk modulus (GPa)	137.90	137.25 [23] 138.50 [24] 138.89 [25] 137.08 [26]
isothermal bulk modulus (GPa)	133.97	133.27 [23] 134.41 [24] 134.77 [25] 133.17 [26]
adiabatic shear modulus (GPa)	43.26	48.16 [23] 47.54 [24] 47.11 [25] 47.20 [26]
adiabatic Young's modulus (GPa)	117.49	127.83
Poisson's ratio	0.358	0.346
bulk sound velocity ($m\,s^{-1}$)	3928.1	3928
Grüneisen parameter	1.99	1.98

2.2 Multi-Einstein method While the Debye–Grüneisen model is based on a simplification of the phonon DOS, the multi-Einstein method by Jacobs et al. [28] implements more features of it, and additionally takes

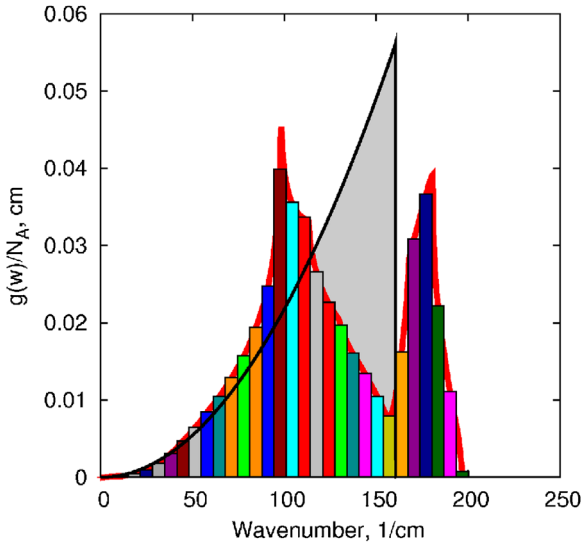

Figure 1 Phonon DOS of Pt obtained by Dutton et al. [29] (red line) and its representation by a 30-Einstein continuum method from Jacobs et al. [28] (coloured bars). The grey area represents a Debye phonon DOS, characterized by a Debye temperature of 234 K obtained with the the Debye–Grüneisen model. N_A represents Avogadro's number.

into account the dispersion of the Grüneisen parameters. The method is semi-empirical in nature, and requires experimental data to constrain the model parameters. It is suitable as an alternative method to construct high-pressure thermodynamic databases applicable in, e.g. mineral physics and geophysics. This allows a significant improvement in the description of the phonon DOS as shown in Fig. 1 for the case of Pt, which is frequently used as pressure reference material in high pressure diamond anvil cell (DAC) measurements. Volume and temperature in a DAC can be measured more accurately and relatively easily compared to determining the pressure. Pressure is derived from the EoS of the pressure reference material (pressure marker), which is inferred to be known accurately. The development of an accurate pressure scale is not trivial and has been the subject of many investigations since 1970 as shown in an overview of Syassen [30]. The thermodynamic analysis of Pt is based on the work of Jacobs et al. [28], in which the pressure scale of Dorogokupets and Oganov [31] has been adopted to constrain the room-temperature V–P isotherm by converting pressures determined by Dewaele et al. [21] in the range of 0–90 GPa. The thermodynamic analysis of experimental 10^5 Pa properties, and the Hugoniot was additionally constrained by the phonon DOS established by Dutton et al. [29] and determined by a combination of inelastic neutron scattering experiments and lattice dynamics. The description of the electronic heat capacity in the thermodynamic analysis is based on first-principles calculations of Tsuchiya and Kawamura [32] in T–V space. The nonlinear behaviour of the electronic isochoric heat capacity, C_V, deduced from these first-principles calculations is not only important for constraining the 10^5 Pa isobaric heat capacity, C_P, between 0 K and the melting point, but also for the representation of data obtained by shock-wave (SW) experiments (Hugoniot). Hugoniot experimental data are crucial in determining the EoS of materials because they cover large ranges of pressure and temperature. These data are obtained by generating SWs in the material to be investigated using detonating explosives or high-velocity projectiles impacting the substance. Points on a Hugoniot curve in V–P space are obtained by shocking the substance with different impact velocities. The positions of these points are expressed by laws of conservation of mass, energy and momentum. An overview of this technique is given by Ahrens [33].

One of the outcomes of the thermodynamic analysis is that the pressure scale determined by Dorogokupets and Oganov [31] is consistent with SW experimental data on the Hugoniot, covering a temperature range between room-temperature and about 13 000 K. To arrive at an accurate representation of experimental SW data on the Hugoniot requires the calculation of all thermodynamic properties, free from unrealistic physical behaviour in them. Figure 2 illustrates that heat capacity and thermal expansivity in P–T space as calculated by the multi-Einstein method meet this requirement. Since thermal expansivity decreases with pressure, the isobaric heat capacity converges at extremely high pressure to the isochoric heat capacity. Although, it is possible to include dispersion in the Grüneisen parameters for different frequency ranges in the multi-Einstein method, Jacobs et al. [28] used an average Grüneisen parameter in their model for platinum, resulting from a least-squares optimization of experimental data. That appeared to be sufficient to represent all thermodynamic data to within experimental uncertainty. Turning to the phonon DOS plotted in Fig. 1, Jacobs et al. [28] used their results to develop a Debye–Grüneisen model for platinum. This was accomplished by fitting the thermodynamic data in a least-squares optimization process, using the same average Grüneisen parameter as in their multi-Einstein model. Additionally, they used the same value for volume, bulk modulus and its pressure derivative for the static lattice and fitted the value for the Debye temperature. In that case, the Debye temperature replaces the model parameters determining the phonon DOS, such as Einstein temperatures and fractions. Although, the phonon DOS of the Debye model differs from that of the multi-Einstein method and the lattice dynamical model of Dutton et al. [29], illustrated in Fig. 1, thermodynamic properties calculated in P–T space, are insignificantly different from those obtained with the multi-Einstein method except for heat capacity in the small temperature range between 15 and 60 K. Despite the small difference in heat capacity, an accurate representation for SW data on the Hugoniot is established and the room-temperature V–P isotherm is insignificantly different from the results obtained with the multi-Einstein method. The Debye–Grüneisen model is therefore, for elements such as platinum, suitable to develop an accurate pressure scale. In the beginning of Section 1.2,

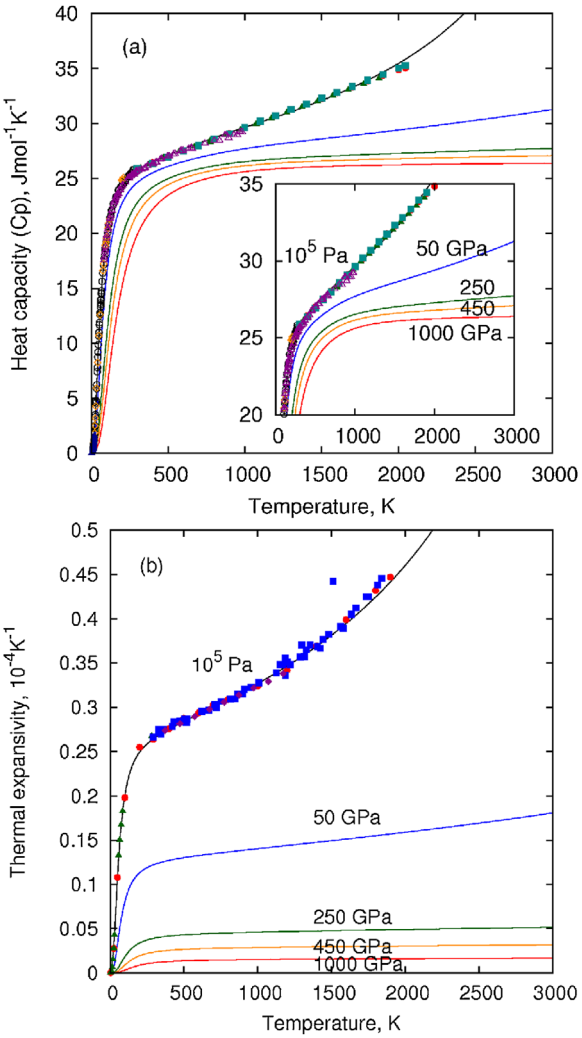

Figure 2 Calculated isobaric heat capacity (a) and thermal expansivity (b) in P–T space for platinum using the multi-Einstein method of Jacobs et al. [28]. The melting temperature of platinum is 2042 K at 10^5 Pa, whereas, according to Belonoshko and Rosengren [34] it is about 4000 K at 50 GPa.

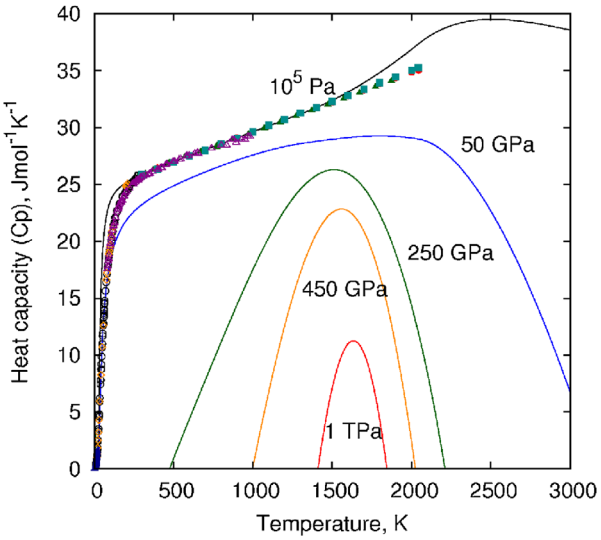

Figure 3 Isobaric heat capacity in P–T space for platinum calculated by a traditional CALPHAD approach using the method by Saxena [7]. The melting temperature of platinum is correctly captured at 10^5 Pa (2042 K) but not at higher pressures.

we stated that it is not a trivial task to derive volume properties from the commonly employed CALPHAD method. In this method, the model parameters are obtained by fitting the 10^5 Pa properties heat capacity, thermal expansivity, and compressibility and the pressure derivative of bulk modulus.

The expression for the Pt isobaric heat capacity was taken from Dinsdale [35]. We used a third order Vinet et al. [36] EoS in the fitting process because the multi-Einstein description employs the same EoS for describing the static lattice properties at 0 K. Because the pressure derivative of the bulk modulus (or compressibility) changes with temperature in the multi-Einstein method, we used the same method as recommended by Saxena [7] to represent this behaviour. The representation of the fitted thermodynamic properties agrees quite well within the experimental uncertainty reported for these properties, and the model description is sufficient to predict the behaviour of thermodynamic properties in P–T space. However, Fig. 3 shows that the derived heat capacity exhibits an unrealistic behaviour, and that it becomes negative at low and high temperatures at pressures above about 50 GPa. This behaviour indicates that the multi-Einstein method cannot deliver in a simple way the key parameters that are required by a model commonly employed in CALPHAD. Therefore, the non-trivial problem arises that thermodynamic databases constructed with the CALPHAD method and applicable at 10^5 Pa pressure, cannot be extended to include pressure in a simple manner. That excludes the method for representing the Hugoniot for platinum and developing a pressure scale. Apparently, other mathematical expressions are needed to incorporate pressure in traditional CALPHAD methods. Because state-of-the-art first-principles methods provide microscopic properties, such as phonon DOS for substances and associated Grüneisen parameters, it is natural to anticipate that thermodynamic methods incorporate them in future thermodynamic analyses of experimental data for constructing databases. Therefore open-source software for using the multi-Einstein method has been developed [37] to assist in developing thermodynamic descriptions for materials, enhancing the application of CALPHAD methodology in multi-disciplinary fields, where pressure is an important property.

A complementary approach, currently developed, is to modify and/or extend the empirical formalism developed by Jacobs and Oonk [38] by using expressions for bulk modulus as function of volume. Alternatively, the CALPHAD method could be extended to incorporate pressure by an empirical method recommended by Brosh et al. [39]. Both empirical methods aim at keeping existing parameterizations for 10^5 Pa thermodynamic properties unchanged, in the development of

a database applicable to, for instance, geophysics. Presently, these methods have the disadvantage that they cannot be constrained by microscopic properties either obtained by spectroscopic experimental techniques or first-principles methods.

3 Experimental data In the assessment of model parameters, various experimental data are collected from the literature. For the case of the Debye–Grüneisen model, useful experimentally measurable properties for Cu are listed in Table 1, as an example. Many of these properties are measured over a wide range of temperature and pressure. Methods based on lattice vibrations, are supported by a physical theory anyway but require experimental data to constrain the model parameters. Additionally, these model parameters can be constrained by values for macroscopic and microscopic properties obtained by first-principles methods.

In the traditional CALPHAD method to construct databases for metallurgical systems at 10^5 Pa pressure, the isobaric heat capacity C_P is a fundamental property and mathematical parametrizations for elements are given in a compilation by Dinsdale [35] (for more details see accompanying Ref. [27]). These parametrizations are kept fixed in any thermodynamic assessment of binary and multi-component systems. Methods incorporating pressure require besides heat capacity, experimental data for volume and its derivatives with respect to temperature and pressure. For elements and many compounds, experimental data for volume (or lattice parameter) and thermal expansivity at 10^5 Pa pressure as function of temperature are available from, e.g. X-ray methods and dilatometry, such as compiled by, e.g. Touloukian et al. [20] or Pearson [40]. Because thermal expansivity is related to Grüneisen parameters of vibrational modes, Raman and infrared spectroscopic measurements of vibrational frequencies in P–T space are useful to constrain its thermodynamic description.

The isothermal bulk modulus associated with the inverse of the pressure derivative of volume is mostly indirectly determined by measuring the adiabatic bulk modulus. The Adiabatic bulk modulus K_S, which is related to isothermal bulk modulus, K, by the simple expression $K_S = KC_P/C_V$ is derived from measurements of the longitudinal and shear sound wave velocities in different crystallographic directions, such as in Brillouin scattering experiments or by using ultrasonic pulse-echo techniques. In combination with volume–pressure–temperature measurements carried out in DACs, these data are useful for constraining the EoS of a material. For substances having a large stability range in P–T space, Hugoniot data (shock waves) are indispensable to further constrain the EoS. This is especially important for substances used as pressure reference materials. Saxena and Wang [41] give an overview on high pressure experimental methods.

4 Elastic constants

4.1 Calculation First-principles calculations can not only provide phonon DOS but also the values of elastic constants for arbitrary crystal structures. To this end, density-functional theory (DFT) is a powerful tool to complement experiment in cases where no experimental values are available (yet) or hardly accessible due to, e.g. metastable phases. The experimental techniques to obtain elastic constants are summarized, e.g. in Refs. [42, 43]. The DFT calculations make use of the expansion of the total energy of a solid at zero stress and equilibrium volume V_0 in small strains $\boldsymbol{\epsilon}$

$$E(\boldsymbol{\epsilon}) = E(0) + \frac{1}{2!} V_0 \sum_{ijkl} \epsilon_{ij} C_{ijkl} \epsilon_{kl} + \ldots \tag{1}$$

with indices i, j, k, l ranging from 1 to 3. The symmetric strain tensors C_{ijkl} are commonly expressed by Voigt notation with two indices C_{ij} that range from 1 to 6. In the following, we restrict the discussion to linear elastic behaviour, i.e. to stress that varies linearly with strain. The number of independent elastic constants C_{ij} is determined by the symmetry of the crystal with a maximum value of 21 for triclinic lattices. The symmetry of the Bravais lattices reduce this number to nine for orthorhombic lattices, five for hexagonal lattices, and 13 for monoclinic lattices. Cubic lattices have three independent elastic constants (C_{11}, C_{12} and C_{44}), tetragonal lattices have six elastic independent elastic constants. The numerical values of the independent elastic constants can be computed by identifying the analytic expression for the second derivative of Eq. (1) with respect to an applied strain δ with the numerical value of the second derivative of the total energy obtained from first-principles calculations of unit cells that are exerted to suitable strain tensors. As an example, consider the orthorhombic deformation of a cubic unit cell

$$\boldsymbol{\epsilon} = \begin{pmatrix} \delta & 0 & 0 \\ 0 & -\delta & 0 \\ 0 & 0 & \delta^2/(1-\delta^2) \end{pmatrix}. \tag{2}$$

Here, the numerical derivative of the total energy with respect to δ equals $V(C_{11} - C_{12})\delta^2$. The full set of independent elastic constants is then obtained by setting up a set of similar equations for an appropriate choice of independent deformations and computing the respective numerical derivatives with respect to δ. The set of independent deformations is not uniquely defined but there are well-established examples in literature [44–46] and systematic approaches have been proposed to compute the elastic constants within the same scheme for arbitrary crystal symmetry, see, e.g. Ref. [47]. In some cases, the number of required deformations can be reduced to fewer than the number of inequivalent elastic constants [48]. Equivalent schemes hold for computing higher-order elastic constants, see, e.g. Ref. [49].

The numerical calculation of elastic constants with atomistic approaches is prone to uncertainties even for the case of first-principles calculations. Besides systematic errors that may arise from choosing deformation sets that violate the volume conservation, there are variations for different

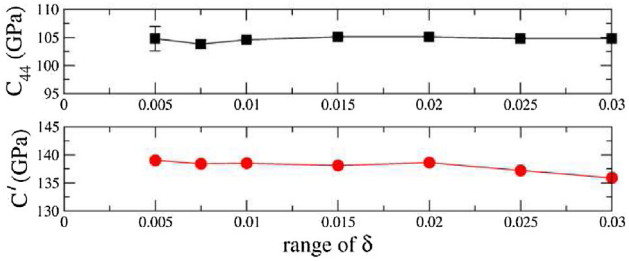

Figure 4 Variation of the computed values of C_{44} and C' for bcc Fe with different magnitudes of applied strain δ. Each strain interval $[-\delta,\delta]$ is sampled by a series of calculations, the computed total energies are fitted to the analytic second derivative of Eq. (1). (Reprinted figure from Ref. [50]. Copyright (2011) by Elsevier.)

exchange-correlation functionals and basis-sets. The computed values of the independent elastic constants may additionally vary with the applied magnitude of strain δ as demonstrated e.g. for the case of C_{44} and $C' = (C_{11} - C_{12})/2$ of bcc Fe [50] (Fig. 4). The value of δ is usually chosen as a compromise of the numerical precision needed to compute the elastic response to small deformations and the onset of nonlinear elastic response at larger deformations of a few percent in strain [51]. Larger values of strain in particular directions lead to the well-known transfomation paths to other crystal structures that are additionally affected by the magnetic ordering in bcc Fe [52].

4.2 Variation with pressure A similar procedure holds for computing the elastic properties of systems under pressure. The total energy at a volume V that corresponds to a strained reference volume V^{ref} is given by [53]

$$E(V,\boldsymbol{\epsilon}) = E(V^{\mathrm{ref}},\boldsymbol{\epsilon}=0) + V^{\mathrm{ref}}\sum_{ij}\sigma_{ij}\epsilon_{ij} + \frac{V^{\mathrm{ref}}}{2}\sum_{ijkl}\epsilon_{ij}C_{ijkl}(V^{\mathrm{ref}})\epsilon_{kl} + \ldots \quad (3)$$

with an additional term to Eq. (1) that is first-order in strain and corresponds to hydrostatic stress σ_{ij}. The energy-strain coefficients C_{ijkl} of the strained system are no longer equal to the stress–strain coefficients $\overset{\circ}{c}_{ijkl}$ of the equilibrium system [53, 54] but transform with the pressure P as [55]

$$\overset{\circ}{c}_{ijkl} = C_{ijkl}(V^{\mathrm{ref}}) + \frac{1}{2}P\left(2\delta_{ij}\delta_{kl} - \delta_{il}\delta_{jk} - \delta_{ik}\delta_{jl}\right). \quad (4)$$

Experimental measurements of elastic constants with ultrasonic wave-propagation [56] or diffraction techniques [57, 58] determine the pressure-varying elastic constants from stress–strain relations.

In the case of Fe, the stress–strain coefficients vary linearly with hydrostatic strain for fcc and hcp [59], as well as for bcc [50] as shown in Fig. 5. However, there can be significant deviations from a simple linear behaviour as has been observed, e.g. for the case of pure vanadium [60–62], see Fig. 6. The challenge for thermodynamic databases is clearly

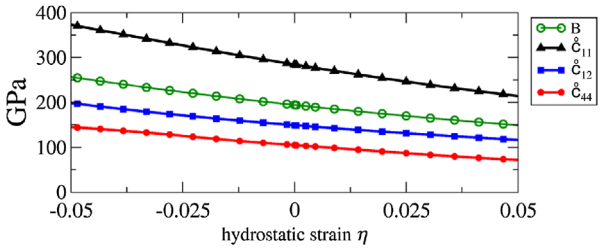

Figure 5 Stress–strain coefficients for pure bcc Fe as obtained from DFT calculations [50] for different hydrostatic strain $\eta = \Delta V/V_0$ relative to the equilibrium volume V_0. (Reprinted figure from Ref. [50]. Copyright (2011) by Elsevier.)

to cast these qualitatively different behaviours in a consistent functional form that is able to account for nonlinear variations of the stress–strain coefficients with pressure.

4.3 Variation with temperature For many systems at temperatures below the melting temperature T_{m} the dependence of elastic constants on T can be fitted to the following empirical relation [63]:

$$C_{ij}(T) = \left[1 - bT\exp\left(-\frac{T_0}{T}\right)\right]C_{ij}(0) \quad (5)$$

where b is a constant and T_0 is of the order of 1/3 of the Debye temperature Θ_{D}. Anomalous temperature dependence is also possible, where a violation of Eq. (5) can be caused by electronic structure effects, see, e.g. Ref. [64] for the case of bcc Fe. For temperatures $T_0 \ll T$ the leading terms in Eq. (5) are

$$C_{ij}(T) = [1 - b\,(T - T_0)]\,C_{ij}(0) \quad (6)$$

which is linear in T. Close to the melting temperature, high-order anharmonic effects usually give a stronger temperature dependence than linear in T [63].

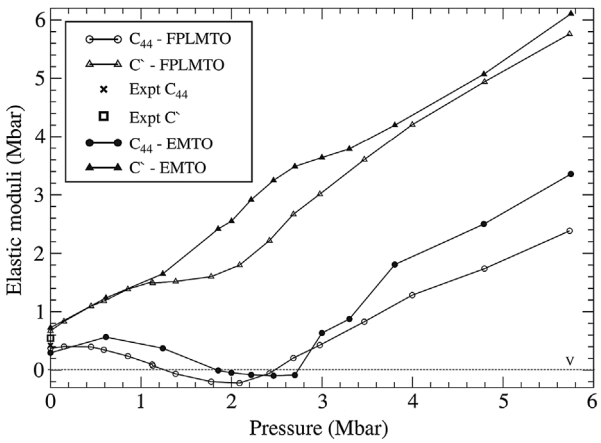

Figure 6 Calculated stress–strain coefficients for pure bcc vanadium as a function of pressure P. (Reprinted from [60], Copyright (2006), with permission from Elsevier.)

First-principles calculations of elastic constants are most often carried out at $T = 0$ K for a static lattice, i.e. without including vibrational effects. However, even at low temperatures the lattice dynamics may give significant contribution to compressibility of light elements due to the relatively high importance of zero point motion of ions. For example in Ref. [65] it was shown that the phonon contribution has a profound effect on the EoS of the high-pressure phase of boron, γ-B or B_{28}, giving rise to anomalously low values of the pressure derivative of the bulk modulus and greatly improving the agreement between theory and experiment. Unfortunately, several approximations within the first-principles approach, like different choices for exchange-correlation functionals within DFT, lead to up to 10% uncertainty for the calculated elastic constants anyhow. Moreover, because the anharmonic effects determine the behaviour of elastic constants at high temperature, the most consistent way to simulate the high-temperature regime from first-principles is based on *ab initio* molecular dynamics (AIMD) [66], which is time consuming. Because the increase in computational efforts required for the treatment of finite temperature effects in calculations of elastic constants is substantial, only few studies have been carried out so far. One case where the importance of temperature effects is well recognized in simulations of elasticity is given by studies of Fe at extreme conditions in the Earth's core [67, 68]. At the same time, even for construction and functional materials the temperature conditions at which they are synthesized and/or operate are often extreme. This influences their elasticity. For example in Ref. [66] the elastic properties of cubic TiN, a parent material for many alloys used for hard coatings of, e.g. cutting tools, have been studied theoretically in a wide temperature interval. A strong dependence of C_{11} and C_{44} elastic constants on temperature has been predicted. For instance, C_{11} has decreased by more than 29 % at 1800 K as compared to its value obtained at $T = 0$ K. Strong temperature dependence of elastic anisotropy of TiN has been observed as well; the material becomes substantially more isotropic at high temperatures, characteristic for cutting tools operations, as well as for phase transitions upon annealing. Thus, the importance of taking into account finite temperature effects in theoretical calculations of elastic properties of materials may be higher than one believes at present, especially for materials intended for high-temperature applications or for simulation of phase transitions at elevated temperatures.

It is also important to point out that in magnetic materials temperature can influence the elastic properties via the magnetic state. When the temperature increases above the Curie temperature (for ferromagnetic systems) or Neel temperature (for antiferromagnetic systems), the magnetic moments most often are not quenched, but become disordered, leading to modifications of the elastic response of the system. This is a well-known effect that has been confirmed in recent first-principles calculations for different materials, e.g. high-strength Fe–Mn steels [69] and CrN [70]. A consistent treatment of the combined effects of lattice vibrations and magnetic disorder represents a highly non-trivial task.

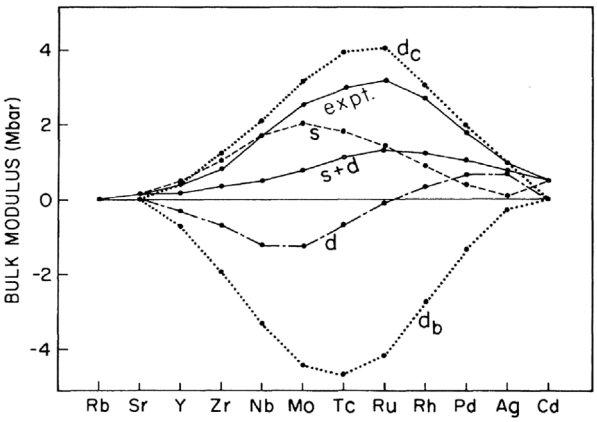

Figure 7 Trend of the bulk modulus with band filling across the transition-metal series. The computed bulk moduli (labeled $s + d$, taken from Ref. [72]) as compared to experiment (expt., taken out of Ref. [73]). The individual contributions of the free electron energy (s), the d-band energy (d_b) and its shift of the band-center (d_c) are indicated. The curve labeled with d refers to the sum of the d_b and d_c contributions. (Reprinted figure with permission from [72]. Copyright (1983) by the American Physical Society.)

The disordered local moment molecular dynamics has been proposed by Steneteg et al. [71] and successfully applied for calculations of equations of state of antiferromagnetic orthorhombic and paramagnetic cubic phases of CrN, but more work is clearly needed in this direction.

4.4 Variation with composition In addition to the variation of the elastic response of elements with pressure and temperature, there are also effects due to chemical composition. A first approach to an understanding of the variation of elastic response with chemical composition is the variation for elemental systems. Early investigations [72] showed that the trend of bulk moduli across the transition-metal series can be largely captured by approximate electronic structure methods, see Fig. 7. The trend is in very good agreement with experiment given that only free-atom properties (pseudopotential core radius, d-state radius and relative number of s and d electrons) are used and was later confirmed with tight-binding calculations for fcc and hcp transition metals [74].

For compound systems, the situation is more complex and here we distinguish between (i) dilute alloys, (ii) ordered alloys and (iii) disordered alloys. The elastic constants of dilute alloys can be easily computed by treating the dilute component as point defect in the unit cell of the majority component as host material. With increasing concentration, the presence of point defects can cause a distortion of the host lattice [75] that lowers the lattice symmetry and hence increases the number of independent elastic constants. For low concentrations, however, it is usually a good approximation to compute the elastic constants under the assumption of preserved crystal symmetry as shown, e.g. for up to 11 at.% of interstitial H atoms in bcc Fe [50]. A related peculiarity in atomistic calculations is that different breaking of the crystal symmetry by different arrangements of point defects lead to

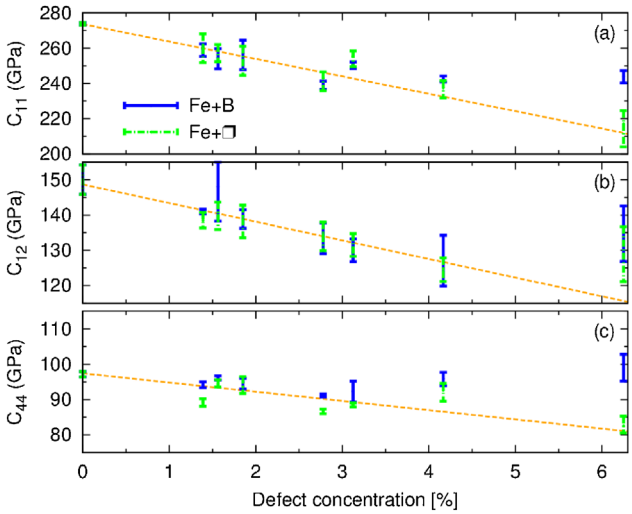

Figure 8 Elastic constants (a) C_{11} , (b) C_{12} and (c) C_{44} for bcc Fe as function of B and vacancy concentration as obtained from DFT calculations [76]. The error bars were estimated by comparing second-, third- and fourth-order polynomials for the fit. (Reprinted figure from Ref. [76]. Copyright (2013) by the American Physical Society.)

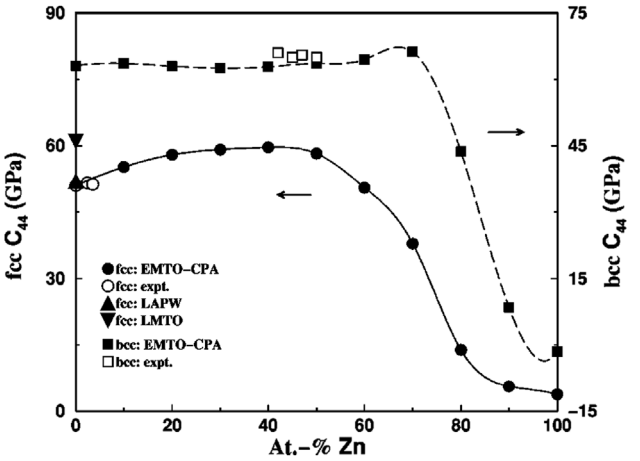

Figure 9 Elastic anomalies of the elastic constant C_{44} of fcc-based Ag–Zn alloys [85]. (Reprinted figure with permission from [85]. Copyright (2002) by the American Physical Society.)

a variation of the elastic constants even at the same point-defect concentration. The variation of the elastic constants with defect concentration is often linear, e.g. for interstitial H [50] or for vacancies in bcc Fe [76]. However, there are also cases with nonlinear variation such as substitutional B atoms in bcc Fe already at low concentrations, see Fig. 8, that may be attributed to the formation of chain-like arrangements of point defects [76].

The treatment of disorder is somewhat opposed to the periodic boundary conditions that are usually used in DFT calculations for bulk systems. Common approaches to properly incorporate the effect of disorder are the coherent-potential approximation (CPA) [77, 78], the cluster expansion (CE) method [79] and special quasi-random structures (SQS) [80]. While initially developed to determine the structural stability of disordered systems, the CPA [81], CE [82] and SQS [48, 83] methods have also been adapted to compute the elastic constants in disordered alloys. The computation of elastic constants with CPA based on electronic-structure calculations was carried out, e.g. for bcc-based Fe–Mg and Fe–Cr disordered alloys [84], and showed very good agreement with experimental values. It could be shown that Mg has a larger impact on the elastic constants of Fe-based alloys than Cr, while Cr showed an anomalous variation of elastic properties at low concentrations. Such nonlinear variations of elastic properties with chemical composition have also been observed in other materials, including changes as drastic as shown for fcc-based Ag–Zn alloys [85] in Fig. 9. The difference of elastic constants between ordered and disordered structures with the same chemical composition can be up to 50% as shown for fcc-based Al–Ti alloys with an SQS approach [83].

5 High-pressure melting In extension to the stable and metastable crystal structures discussed above, we will consider the effect of pressure on lattice stability. The complexity of pressure effects described above for zero temperature is further increased for temperatures close to the melting point. High pressure melting is controversial for a number of elements, especially transition metals but also alkali metals. As an example, we discuss here the case of iron, which is a particularly important case because the Earth's core is mainly made by iron. The core is solid at the centre of the Earth, with a central pressure of 364 GPa. At a distance of 1220 km from the centre it becomes liquid, and the pressure is 329 GPa. The solid–liquid boundary must be at the melting temperature, and therefore knowledge of the melting temperature of iron at 329 GPa provides a proxy for the temperature of the core. At low pressure, it is possible to perform DAC experiments [86–92]. Above ∼200 GPa only SW experiments are available [93–95]. Because of the extreme conditions, experiments are not easy to perform, and a large scatter of data from different groups is apparent. Towards the end of the last century, a number of calculations based on first-principles techniques became available using different approaches: Laio et al. [96] and Belonoshko et al. [97] fitted a classical potential to first-principles data within the DFT formalism, and then used the classical potential to obtain the melting curve in the whole pressure range relevant to the Earth's core. The results of the two groups did not agree with each other, which was not surprising as the two classical potentials used by them were not the same.

Alfè et al. [98–100] computed the Gibbs energies of solid and liquid iron using DFT, and found the melting curve from the thermodynamic relation $G_l(P, T) = G_s(P, T)$, where $G_l(P, T)$ and $G_s(P, T)$ are the Gibbs energy of the liquid and the solid, respectively, at pressure P and temperature T. The free energies were calculated using the thermodynamic integration method, which is a standard statistical mechanics approach that allows to compute free energy differences

between two systems. The main idea of the method is that one first calculates the energy of a reference system, typically an empirical potential, and then the free energy difference between the *ab initio* system and the reference system $\Delta F = \int_0^1 \mathrm{d}\lambda \langle U - U_{\mathrm{ref}} \rangle_\lambda$, where U and U_{ref} are the potential energy functions of the *ab initio* and the reference system, respectively, and $\langle \cdot \rangle_\lambda$ means canonical average in the ensemble generated by $U_\lambda = \lambda U + (1-\lambda) U_{\mathrm{ref}}$. Canonical averages are usually calculated using the molecular dynamics method. If the reference system is appropriately chosen, then ΔF can be calculated efficiently with short simulations and using relatively small systems of $\simeq$100 atoms. Once the Helmholtz energy F is known, the Gibbs energy can be easily constructed from the thermodynamic relation $G = F + PV$.

The melting curve of Alfè et al. [100] was different from those of Laio et al. [96] and Belonoshko et al. [97]. The reason for these discrepancies was investigated by Alfè et al. [101], and was found in the energy difference between DFT and the model used by the two other groups. This is easily understood by picturing the thermodynamic relation, which defines the melting point, namely the crossing of the free energy of the liquid G_{s} and that of the solid G_{l}. If there is a relative shift of G_{l} with respect to G_{s} when DFT is replaced with a model potential, then the point where $G_{\mathrm{l}} = G_{\mathrm{s}}$ will be different. It is easy to show that, if the relative shift of free energy is not too large, the shift of melting temperature δT_{m} can be expressed as $\delta T_{\mathrm{m}} \simeq (\Delta G_{\mathrm{l}} - \Delta G_{\mathrm{s}})/S^{\mathrm{ls}}$, where ΔG_{l} and ΔG_{s} are the free energy differences between DFT and the model for liquid and solid, respectively, and S^{ls} is the entropy of melting. By computing these free energy differences between DFT and the model employed by Belonoshko et al., it was possible to reconcile the melting curves computed by Alfè et al. [100] and Belonoshko et al. [97].

An alternative statistical mechanics approach to the calculation of the melting temperature is the so called coexistence method. Here solid and liquid are simulated side by side in the same box, and the melting point can be extracted directly from the simulation. If the calculations are done in the NVE ensemble (N is the number of particles, V the volume of the system and E the internal energy), then for every chosen value of V there is a whole range of internal energies E for which solid–liquid coexistence is maintained, and the average of the instantaneous temperature T and pressure P over the course of the simulation provides a point on the melting curve. The method is intrinsically more expensive than the Gibbs energy approach, as systems containing at least 1000 atoms are typically needed. This is roughly one order of magnitude bigger than the size of the systems employed in the free energy approach, and therefore the method is very expensive if used in conjunction with DFT. However, it is an independent approach, which gives the same answer as the Gibbs energy method if the same technical parameters are used. The method was recently used to compute a point on the melting curve of iron [102], and indeed produced a result compatible with those obtained with the free energy method.

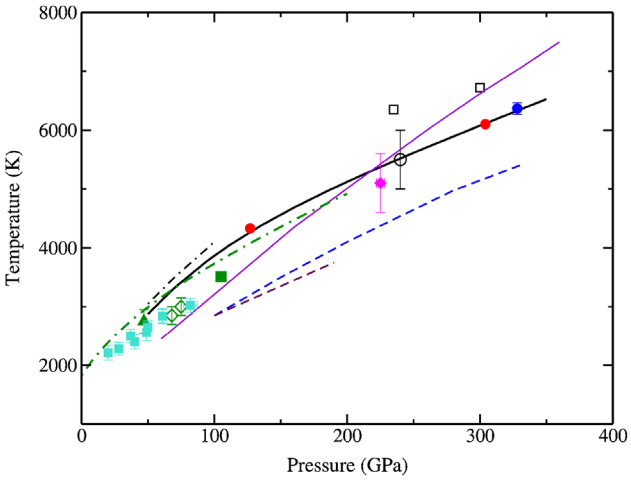

Figure 10 Comparison of melting curve of Fe from DFT calculations and experimental data: black solid curve: first-principles results of Ref. [100]; blue filled dot: first-principles coexistence result of Ref. [102]; red filled circles: corrected coexistence results from Ref. [101]; blue dashed curve: empirical potential results of Ref. [96]; purple curve: empirical potential results of Ref. [97]; black chained and maroon dashed curves: DAC measurements of Refs. [86] and [88]; green diamonds and green filled square: DAC measurements of Ref. [89] and Ref. [90]; magenta filled squares: DAC measurements of Ref. [91]; green chained line: DAC measurements of Ref. [92]; black open squares, black open circle and magenta diamond: shock experiments of Refs. [95], [93] and [94]. Error bars are those quoted in original references.

The ultimate test of a theoretical prediction is experimental verification, and although at the time of writing the exact value of the melting curve of iron at the Earth's inner core conditions remains a prediction, new experiments in the pressure range 50–200 GPa [92] fully confirm the DFT melting curve [100] in this pressure range. This shows how first-principles calculations have now reached a degree of reliability that is comparable to experiments, and can be used to predict thermodynamic properties of matter under a wide range of pressure–temperature conditions. A comparison of measured and calculated melting curves of iron is displayed in Fig. 10.

6 Magnetism The influence of magnetism on thermodynamic functions is discussed in detail in Ref. [103]. Here we consider the effect of pressure on magnetic properties of elements having itinerant magnetic moments, like 3d transition metals and their alloys and compounds. The magnetic moments in this case are formed by quite localized d-electron states with a bandwidth of 3–4 eV. A phenomenological understanding of the influence of pressure on their magnetic properties at zero temperature can be obtained within the Stoner theory, which relates the presence of (ferro-)magnetic instability to the value of the electronic density of states (DOS) at the Fermi energy, $N(E_{\mathrm{F}})$:

$$IN(E_{\mathrm{F}}) > 1 \tag{7}$$

where I denotes the so-called Stoner parameter. The Stoner criterion states that ferromagnetism appears when the gain in exchange energy is larger than the loss in kinetic energy.

High DOS indicates a tendency towards the appearance of local magnetic moments and towards their ordering. By compression one reduces interatomic distances, which results in a broadening of the bands, generally leading to a decrease of the DOS at E_F. Because the Stoner parameter is an intra-atomic quantity and is known to depend only little on crystal environment, the decrease of $N(E_F)$ favours the suppression of both magnitudes of local magnetic moments and the order between them. However, despite this simple picture there are surprises. In particular, Fe has a robust magnetic moment of $\sim 2.1\mu_B$ at ambient conditions, while Ni has a highly itinerant magnetic moment of $\sim 0.6\mu_B$. However, the magnetic moment in Fe is quenched already at $\sim$ 18 GPa upon the phase transition from the bcc to the hcp phase [104]. At the same time, very recent experiments demonstrate, that the magnetic moment in Ni survives at least up to 200 GPa, and the theory predicts the disappearance of magnetism in Ni to occur above 400 GPa [105].

Considering a combined influence of pressure and temperature on the magnetic properties of transition metals, one has to complement the Stoner picture at zero temperature with the Heisenberg model description of interactions between magnetic moments. It is generally believed that a magnetic structure in transition-metal alloys with itinerant magnetic moments may still be satisfactorily described as a classical Heisenberg system with local moments centred at the sites of the crystal lattice [106]. In the absence of an external magnetic field, this allows the exchange interactions in the systems to be characterized by the model Hamiltonian

$$H_{\mathrm{mag}} = -\sum_{i,j\neq i} J_{ij} e_i e_j \qquad (8)$$

where J_{ij} are the pair exchange interaction parameters (see Fig. 11) and e_i is the unit vector in the direction of the magnetic moment at site i. In general, J_{ij} depends on the distance between atoms. For example in fcc Fe this dependence is particularly strong [108]. Therefore, both the strength of the interactions and the degree and type of magnetic order can be influenced by pressure. Even stronger influence on J_{ij} can be achieved via variation of the occupation of the transition metal d-band (Fig. 11) [107]. This can be done, e.g. by alloying, opening up new opportunities for basic research and for the design of new materials with special properties. For example the so-called Invar Fe–Ni alloys do not expand with temperature, but the range of composition is very narrow, $\sim$35 to 38 at.% Ni. By application of pressure Dubrovinsky et al. [109] broadened this interval to alloys with up to 80 at.% Ni.

The properties of magnetic metals depend on temperature, external field and volume. The two former are relatively easy to vary in the laboratory, and therefore they are broadly used in experimental studies. The latter can be changed by application of pressure, but this requires special facilities for experiments. In fact, there are only two established methods of studying magnetism in solids under pressure; neutron diffraction and XMCD or Mössbauer effect-based spectroscopies. While neutron diffraction is probably the most powerful tool for studies of magnetism, the pressure range of experiments is currently limited to few tens of GPa for materials containing species with high magnetic moments. The XMCD studies have just been extended to over 200 GPa [105], but they are still limited to ferromagnetic compounds. Therefore, investigations of magnetism and magnetic materials under pressures above 10 GPa (and especially under pressure and variable temperatures) are still very limited.

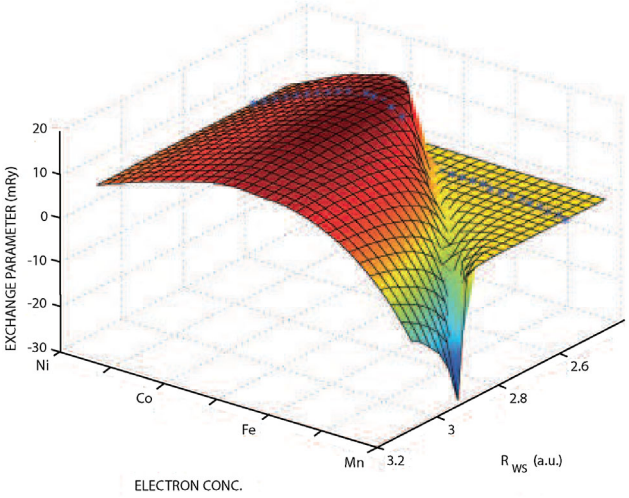

Figure 11 Effective exchange parameter across the fcc 3d-transition-metal series as a function of lattice spacing given by the Wigner–Seitz radius R_{WS} and valence-band occupation in the interval between Mn and Ni [107].

On the other hand, first-principles computer simulations of materials properties based on DFT [110] can provide accurate quantitative descriptions of magnetic materials upon pressure variation without any adjustable parameters fitted to experiments. In particular, net magnetic moments for Fe, Co and Ni as a function of pressure and crystal structure have been calculated by several groups [104, 111]. In Ref. [111], the magnetic effects were also correlated to modifications of thermodynamic properties, like potential energies, lattice parameters and bulk moduli. Körmann et al. [112] studied the influence of pressure on the Curie temperature of bcc Fe. Sha and Cohen [113] investigated finite-temperature magnetism in bcc Fe under compression, and computed the magnetic susceptibility, the Curie temperature, heat capacity and magnetic free energy. Xie et al. [114] calculated high-pressure thermodynamic, electronic and magnetic properties of Ni. They obtained the P–V–T EoS from the Helmholtz energy of the crystal in the quasiharmonic approximation, as well as the pressure dependence of the thermal expansion coefficient, bulk modulus, electronic band structure, phonon spectrum and the magnetic moment.

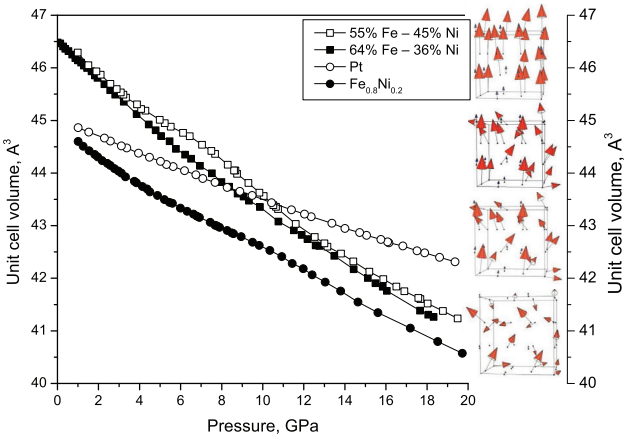

Figure 12 Dependence of volume on pressure for fcc Fe–Ni alloys with different concentrations from Ref. [109]. Pronounced peculiarities are clearly seen for $Fe_{0.55}Ni_{0.45}$ between 5 and 9 GPa, and for $Fe_{0.20}Ni_{0.80}$ between 9 and 14 GPa. A less clear peculiarity may be present for the prototype Invar $Fe_{0.64}Ni_{0.36}$ alloy between ambient pressure and 3 GPa. *P–V* relations for Pt taken in the same experiment and shown in the figure demonstrate smooth variations of volume with pressure and confirm that peculiarities of compression curves of Fe–Ni alloys are related to their properties at high pressure and not to the experimental technique. The sketch to the right shows the evolution of the magnetic structure of the Invar alloy with decreasing volume (or increasing pressure) as calculated in Ref. [117].

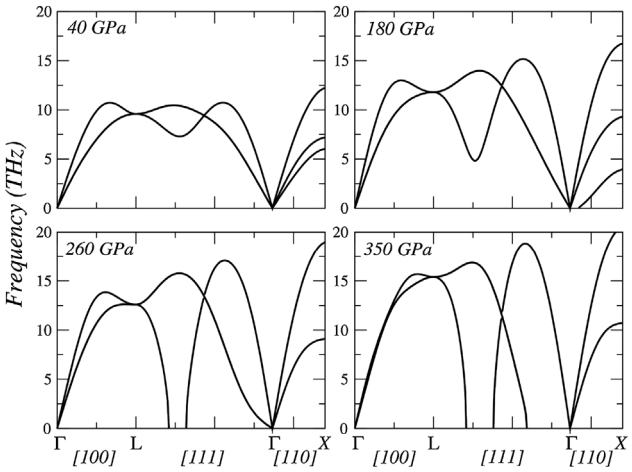

Figure 13 Phonon dispersions of bcc iron at various pressures. Reprinted from Ref. [127].

The calculated results were found to be in good agreement with the available experimental measurements.

At the same time, the calculations most often use certain approximations, which may have limited applicability. In particular, most calculations assume collinear ferromagnetic (or anti-ferromagnetic) order of local moments. While this approximation should be valid for the description of bcc Fe, hcp Co and fcc Ni up to very high pressure at low temperature, it would be quite questionable for the description of fcc Fe and Fe–Ni alloys. Indeed, experiment and theory agree that fcc Fe has a non-collinear magnetic structure at ambient conditions [115, 116], while Fe–Ni alloys are predicted to develop it at high-pressure (Fig. 12) [117]. Temperature-induced magnetic excitations must be considered at elevated temperature for a proper description of phase relations [118]. However, state-of-the-art DFT approaches may be insufficient. For instance, recent theoretical work showed that a collinear antiferromagnetic state (AFM-II) [119, 120] or a more complex AFM state [121] have lower energy than the nonmagnetic state for hcp Fe. Moreover, computations on the AFM-II phase were used to improve the agreement between the calculated and measured EoS of hcp Fe [119, 120]. Nevertheless, the AFM-II phase was not resolved in Mössbauer experiments, and although Ni atoms are predicted to result in an enhancement of magnetic moments on neighbouring Fe atoms, there is no evidence that hcp $Fe_{0.9}Ni_{0.1}$ is a static antiferromagnet down to 11 K at 21 GPa [122].

The theory of magnetism is under constant development. New approaches, like the dynamical mean field theory (DMFT) [123, 124] are proposed to treat many-electron effects essential for a proper description of transition metals magnetism. In particular, the importance of correlation effects in hcp Fe under pressure has been explicitly demonstrated by Glazyrin et al. [125]. A development of first-principles molecular [126] and spin [115] dynamics should allow one to take into account finite-temperature effects in simulations of magnetism under pressure.

7 Dynamical instabilities For a crystal structure to exist at zero temperature, it is necessary that it is dynamically stable, i.e. its phonon frequencies in the Brillouin zone must be all positive. (Phase transitions at higher temperatures are also discussed in the accompanying Refs. [27, 103].) Dynamical instabilities may be driven by pressure, as is the case, for example for bcc Fe at high pressure [127]. For bcc Fe, a dynamical instability appears above a pressure of ∼200 GPa, as the phonon dispersion curves plotted in Fig. 13 show. Therefore, the bcc crystal structure does not exist above this pressure at zero temperature. The instability manifests itself in a maximum of the potential energy function, and drives the system to the ω phase. However, even if the system is unstable at low temperature, it may still be possible that it is entropically stabilized at high temperature. A one-dimensional classic example of this is a symmetric two-well potential: at low temperature the system will break the symmetry and fall into one of the two minima on either side of the central point, but if the temperature is high enough it will sample both regions, and on average it will stay around the central point. This is exactly what happens with bcc Fe at high pressure. If the temperature is high enough the structure becomes dynamically stable. A convenient tool to establish if a crystal structure is dynamically stable at high temperature is the position autocorrelation function, defined as

$$p(t) = \langle(\mathbf{r}_i(t + t_0) - \mathbf{R}_i) \cdot (\mathbf{r}_i(t_0) - \mathbf{R}_i)\rangle, \quad (9)$$

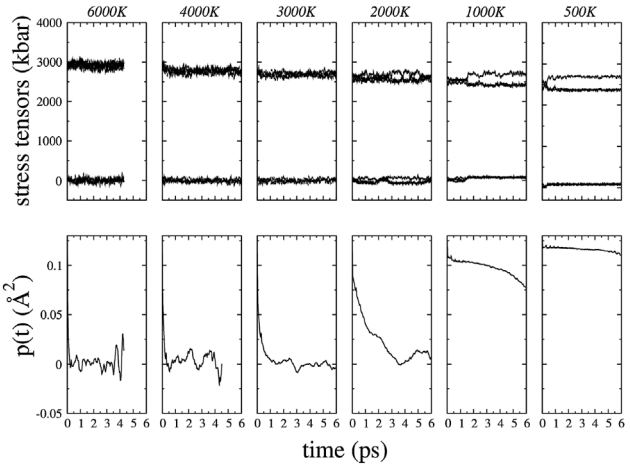

Figure 14 The calculated stress tensors as a function of simulation time (upper row) and position correlation functions (lower row) for a 64-atom cubic supercell of bcc iron at different temperatures. Reprinted from Ref. [127].

where $\mathbf{r}_i$ is the time-varying position of the atom and $\mathbf{R}_i$ is the position of that atom in the perfect bcc structure. The angular brackets denote the thermal average, which in practice is evaluated as an average over time origins, t_0, and atoms i. For long times t, vibrational displacements become uncorrelated, so that $p(t) \rightarrow \langle \mathbf{r}_i - \mathbf{R}_i \rangle^2$, and if all atoms vibrate about bcc lattice sites, $\langle \mathbf{r}_i - \mathbf{R}_i \rangle = 0$, so that $p(t) \rightarrow 0$ as $t \rightarrow \infty$. In Fig. 14, we show the behaviour of $p(t)$ for bcc Fe at high pressure at several temperatures [127]. It is clear that at low temperature $p(t)$ converges to a value above zero, and therefore the bcc structure is dynamically unstable. However, for temperatures above ~ 3000 K the limiting value of $p(t)$ is zero, which indicates that the structure has become dynamically stable. In Fig. 14, we also display the stress tensor of the system, computed along a molecular dynamics simulation performed at constant cell shape with the system in the bcc structure. Below $\sim$3000 K, the stress tensor becomes anisotropic, again indicating departure from dynamical stability. Dynamical stability does not mean, of course, that the structure is also thermodynamically stable. For bcc Fe at the Earth's core conditions, for example the bcc structure has a higher free energy than the hcp structure, and therefore it is still thermodynamically unstable.

The example above is highly relevant for the on-going discussion on one of the most important concepts within the CALPHAD formalism: the lattice stability. It is defined as the difference in Gibbs energies for a pure element based on two different phases, e.g. crystalline structures [128, 129]. However, when an element is dynamically unstable in a certain crystal structure, some vibrational modes at certain wave vectors $\boldsymbol{k}$ have imaginary frequencies, and therefore any distortion of the lattice corresponding to such a vibration would destroy the crystal lattice [130, 131]. For example at the latest Ringberg workshop it was considered that a dynamical instability prevented a meaningful use of the energetics calculated by first-principles techniques, unless the lattice stability is associated with a metastable phase, and not an unstable one [132].

However, as has been demonstrated above for the case of bcc Fe at high pressure, dynamically unstable structures can be stabilized by the anharmonic effects at high temperature. As a matter of fact, this is exactly the mechanism that stabilizes, for instance, Ti, Zr and Hf in the bcc structure at ambient pressure and high temperature [133]. Using Mo as a model system, Asker et al. [134] demonstrated by means of first-principles molecular dynamics simulations that the configurational energy difference between the stable bcc phase and fcc phase, unstable at $T = 0$ K, but stabilized dynamically at high temperature, approaches the value derived by means of the thermochemical approach. A similar conclusion was obtained later by Ozoliņš for W [135]. Several methodologies for calculations of free energies and thermodynamic properties of systems, which are dynamically unstable at zero temperature, but are stabilized dynamically at high temperature, have been suggested [133, 135–138]. In particular, using the temperature dependent effective potential method, Hellman et al. calculated pressure–temperature phase diagrams for two highly anharmonic systems, Zr [137] and ^{4}He [138].

8 Implementation and application In the previous sections, we pointed out the complexity that needs to be covered by thermodynamic functions to include the influence of pressure. In whatever way this dependency of pressure or strain is implemented in a thermodynamic model, the accuracy of any such description may not be the same over the whole range of relevant pressures. From this perspective one faces several options for the database design.

(1) Firstly, one might concentrate on databases specialised for a particular pressure range, i.e. high-pressure databases for geological processes, low-pressure databases for technical applications at typically low pressures that can be footed on elastic constants. With this design decision, the users may need to tolerate a lower accuracy for the out-of-focus pressure regimes.
(2) Secondly, both choices could be implemented in parallel with a selection for the use of either made by the user or by the software based on the set boundary conditions. Again, the user needs to be aware of the different descriptions implemented in the database and even if an automatic switch is possible, the (experienced) user should be able to override this.
(3) The third option that comes to mind is a hybrid approach, which makes use of elastic constants for the lower pressure regime but takes into account pressure-dependent properties for the higher-pressure regime. This approach would consider the normal usage of the implemented data – for technical questions the elastic constants are more important, usually in the low pressure region. For geologists, high pressure data are needed, but these do normally not include the elastic data.

While each approach has its drawbacks, the first two cases seem to be most transparent, and leave the user

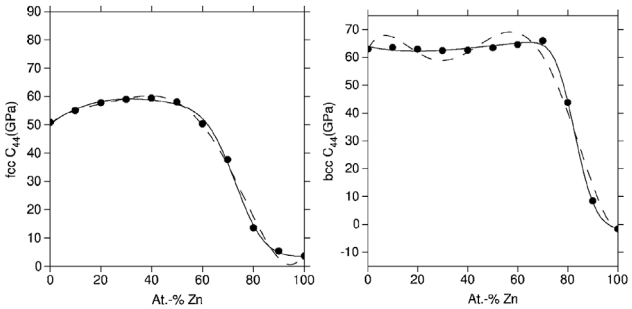

Figure 15 Tentative fit of suggested CALPHAD function to variation of elastic constants with composition for C_{44} of (left) fcc and (right) bcc Ag–Zn. The EMTO-CPA results (points, cf. Fig. 9) are fitted to a fourth order Redlich–Kister polynomial (dashed line) and a second order Redlich–Kister polynomial with an error function (solid line).

some freedom of choice. The major drawbacks of the third approach are an inconsistent material description within the database for different pressure regimes as well as a possibly hindering assumption of the normal usage of the database.

8.1 Extending CALPHAD databases As mentioned by Palumbo et al. [27], the volume for low pressures is already implemented in some databases but not systematically for all phases. Quantities like elastic constants are not used in equilibrium calculations but it is interesting to have them associated to different phases belonging to the database in order to be consistent with the lattice parameters calculated for the selected phase. For example

– LPX(FCC,Cu) is the lattice parameter of fcc Cu,
– C11(FCC,Cu) is the elastic constant C_{11} of fcc Cu.

This can be implemented for any crystal structure (stable or metastable) and these parameters can change with temperature and can be modelled as composition dependent in alloys as shown in the next subsection. These values (like already done for mobilities in some databases) can be exported together with the usual thermodynamic properties to an application software dedicated, for example to phase-field microstructure simulations as MICRESS [139] or Open-Phase [140].

8.2 Composition-dependent elastic constants Here we take the example of the elastic constant C_{44} variation with composition for fcc and bcc Ag–Zn alloys presented in Fig. 9. Using a Redlich–Kister polynomial to accurately describe the composition dependency of the C_{44} is difficult as the end values differ significantly and the curve takes the form of a step. It is then necessary to use a large number of parameters to fit the data. In order to account for the stepwise behaviour of the curve, we instead combined the Redlich–Kister polynomial with an error-function in order to obtain a better fit. Figure 15 shows the result using a fourth order Redlich–Kister polynomial and a second order Redlich–Kister polynomial combined with an error function for the bcc and fcc phase in the Ag–Zn system. This demonstrates exemplarily that the elastic constants can be cast in a simple parametrization even in the case of such nonlinear variations with composition.

9 Conclusions Pressure (or more generally stress) plays a crucial role for structural stability, melting, magnetism and dynamic stability in many systems. Reaching out for the simulation of pressure-driven effects in technical applications therefore calls for an incorporation of strain effects in thermodynamic databases. The existing efforts to realise pressure-dependent databases are still somewhat limited to particular applications and no generally accepted implementation concept seems to be available yet. In this article, we point out that this missing feature of thermodynamic databases is partly due to the multiple effects of pressure on various thermodynamic properties. Even in the low-pressure elastic regime, the often nonlinear variation of elastic constants with pressure, temperature and chemical compositions requires a sophisticated treatment of stress contributions to the free energy. For high-pressures, the situation is further complicated by the complex processes taking place during melting, e.g. from different phases that are stabilized by pressure. The influence of pressure in magnetic systems can lead to additional effects that seem to be hard to cast consistently in a thermodynamic databases (see also the accompanying Ref. [27] on magnetism). This is even more so for dynamical effects that can destabilise phases at low temperatures but stabilise them again at high temperatures. As a conclusion of the identified complex effects of pressure on phase-diagrams, we also suggest a first idea of casting an exemplary nonlinear variation of elastic constants with composition in a simple functional form for usage in thermodynamic databases.

Acknowledgements We are grateful to all participants of the Ringberg meeting for discussions, particularly G. Grimvall, M. Palumbo, M. Sluiter and B. Fultz. T.H., J.K. and S.G.F. acknowledge financial support through ThyssenKrupp AG, Bayer MaterialScience AG, Salzgitter Mannesmann Forschung GmbH, Robert Bosch GmbH, Benteler Stahl/Rohr GmbH, Bayer Technology Services GmbH, the state of North-Rhine Westphalia, the European Commission in the framework of the ERDF and the German Research Foundation (DFG) through projects C1 and C6 of the collaborative research center SFB/TR 103. I.A.A. would like to acknowledge support from the Swedish Research Council (VR) project No. 621-2011-4426, the Swedish Foundation for Strategic Research (SSF) program SRL10-0026. This work was supported in part by the Ministry of Education and Science of the Russian Federation within the framework of the program *Research and Pedagogical Personnel for Innovative Russia (2009–2013)* (project no. 14.B37.21.0890 of 10.09.2012). M.H.G.J. gratefully acknowledges support by the German Research Foundation (DFG) under grant number JA 1985/1. X.G.L. is grateful to the financial support from the National Natural Science Foundation of China (Grant: 51271106).

References

[1] H. Lukas, S. G. Fries, and B. Sundman, Computational Thermodynamics: The CALPHAD Method (Cambridge University Press, Cambridge, 2007).

[2] J. O. Andersson, T. Helander, L. H. Höglund, P. F. Shi, and B. Sundman, Calphad **26**, 273–312 (2002); see also http://www.thermocalc.com/.
[3] C. W. Bale, E. Bélisle, P. Chartrand, S. A. Decterov, G. Eriksson, K. Hack, I. H. Jung, Y. B. Kang, J. Melançon, A. D. Pelton, C. Robelin, and S. Petersen, Calphad **33**, 295–311 (2009); see also http://www.factsage.com/.
[4] V. Knezevic, G. Sauthoff, J. Vilk, G. Inden, A. Schneider, R. Agamennone, W. Blum, Y. Wang, A. Scholz, C. Berger, J. Ehlers, and L. Singheiser, ISIJ Int. **42**, 1505 (2002).
[5] H. J. Rajek, PhD Thesis, Graz University of Technology, Graz, Austria (2005).
[6] Y. Fei, H. K. Mao, and B. O. Myssen, J. Geophys. Res. B **96**, 2157 (1991).
[7] S. K. Saxena, Geochim. Cosmochim. Acta **60**, 2379 (1996).
[8] T. J. B. Holland and R. Powell, J. Metamorph. Geol. **16**, 309 (1998).
[9] O. Fabrichnaya, S. K. Saxena, P. Richet, and E. F. J. Westrum, Thermodynamic Data, Models, and Phase Diagrams in Multicomponent Oxide Systems (Springer, New York, 2004).
[10] X. G. Lu, M. Selleby, and B. Sundman, Calphad **29**, 49 (2005).
[11] A. F. Guillermet, Int. J. Thermophys. **6**, 367 (1985).
[12] M. H. G. Jacobs and H. A. J. Oonk, Phys. Chem. Chem. Phys. **2**, 2641 (2000).
[13] M. H. G. Jacobs, A. P. van den Berg, and B. H. W. S. de Jong, Calphad **30**, 131 (2006).
[14] L. Stixrude and C. Lithgow-Bertelloni, Geophys. J. Int. **2**, 610 (2005).
[15] A. S. Piazzoni, G. Steinle-Neumann, H. P. Bunge, and D. Dolejs, Geochem. Geophys. Geosyst. **8**, 1 (2007).
[16] M. H. G. Jacobs and B. H. W. S. de Jong, Geochim. Cosmochim. Acta **71**, 3630 (2007).
[17] M. H. G. Jacobs and B. H. W. S. de Jong, Phys. Chem. Miner. **36**, 365 (2009).
[18] X. G. Lu, M. Selleby, and B. Sundman, Acta Mater. **53**, 2259 (2005).
[19] X. G. Lu and Q. Chen, Philos. Mag. **89**, 2167 (2009).
[20] Y. S. Touloukian, R. K. Kirby, R. E. Taylor, and P. D. Desai, Thermophysical Properties of Matter: Thermal Expansion, Metallic Elements and Alloys (Plenum, New York, 1975).
[21] A. Dewaele, P. Loubeyre, and M. Mezouar, Phys. Rev. B **70**, 094112 (2004).
[22] W. B. Pearson, The Crystal Chemistry and Physics of Metals and Alloys (John Wiley & Sons, New York, 1972).
[23] P. van't Klooster, N. J. Trappeniers, and S. N. Biwas, Physica B **97**, 65–75 (1979).
[24] Y. A. Chang and L. Himmel, J. Appl. Phys. **37**, 3567–3572 (1966).
[25] R. H. Y. Chang, J. Phys. Chem. **69**, 4162–4165 (1965).
[26] J. G. W. C. Overton, Jr., Phys. Rev. **98**, 969–977 (1955).
[27] M. Palumbo, B. Burton, A. C. de Silva, B. Fultz, B. Grabowski, G. Grimvall, B. Hallstedt, O. Hellmann, B. Lindahl, A. Schneider, P. E. A. Turchi, and W. Xiong, Phys. Status Solidi B **251**, 14–32 (2014), this issue.
[28] M. H. G. Jacobs, R. Schmid-Fetzer, and A. P. van den Berg, Phys. Chem. Miner. **40**, 207 (2013).
[29] D. Dutton, B. N. Brockhouse, and A. P. Miller, Can. J. Phys. **50**, 2915 (1972).
[30] K. Syassen, High Press. Res. **28**, 75–126 (2008).
[31] P. I. Dorogokupets and A. R. Oganov, Phys. Rev. B **75**, 024115 (2007).
[32] T. Tsuchiya and K. Kawamura, Phys. Rev. B **66**, 094115 (2002).
[33] T. J. Ahrens, in: High Pressure Shock Compression of Solids, edited by J. R. Asay and M. Shaninpoor (Springer-Verlag, New York, 1993), p. 75.
[34] A. B. Belonoshko and A. Rosengren, Phys. Rev. B **85**, 174104 (2012).
[35] A. T. Dinsdale, Calphad **15**(4), 317–425 (1991).
[36] P. Vinet, J. Ferrante, J. H. Rose, and J. R. Smith, J. Phys.: Condens. Matter **1**, 1941–1963 (1989).
[37] http://www.opencalphad.org/.
[38] M. H. G. Jacobs and H. A. J. Oonk, Phys. Chem. Miner. **28**, 2379–2395 (2001).
[39] E. Brosh, R. Z. Shneck, and G. Makov, J. Phys. Chem. **69**, 1912–1922 (2008).
[40] W. B. Pearson, Handbook of Lattice Spacings and Structures of Metals and Alloys (Pergamon, New York, 1958).
[41] S. K. Saxena and Y. Wang, in: Methods of Phase Diagram Determination, edited by J. C. Zhao (Elsevier, Oxford, Amsterdam, 2007), p. 412.
[42] H. M. Ledbetter and R. P. Reed, J. Phys. Chem. **2**, 531–617 (1973).
[43] M. Radovic, E. Lara-Curzio, and L. Riester, Mater. Sci. Eng. **A368**, 56–70 (2004).
[44] M. J. Mehl, J. E. Osburn, D. A. Papaconstantopoulos, and B. M. Klein, Phys. Rev. B **41**, 10311 (1990).
[45] T. Kraft, P. M. Marcus, M. Methfessel, and M. Scheffler, Phys. Rev. B **48**, 5886 (1993).
[46] O. Beckstein, J. E. Klepeis, G. L. W. Hart, and O. Pankratov, Phys. Rev. B **63**, 134112 (2001).
[47] Y. LePage and P. Saxe, Phys. Rev. B **63**, 174103 (2001).
[48] F. Tasnádi, M. Odén, and I. A. Abrikosov, Phys. Rev. B **85**, 144112 (2012).
[49] J. Zhao, J. M. Winey, and Y. M. Gupta, Phys. Rev. B **75**, 094105 (2007).
[50] D. Psiachos, T. Hammerschmidt, and R. Drautz, Acta Mater. **59**, 4255 (2011).
[51] T. Hammerschmidt, P. Kratzer, and M. Scheffler, Phys. Rev. B **75**, 235328 (2007).
[52] M. Friak, T. Hickel, F. Körmann, A. Udyansky, A. Dick, J. von Pezold, D. Ma, O. Kim, W. Counts, M. Šob, T. Gebhardt, D. Music, J. Schneider, D. Raabe, and J. Neugebauer, Steel Res. Int. **82**, 86 (2011).
[53] D. C. Wallace, Thermodynamics of Crystals (Dover, New York, 1972).
[54] T. H. K. Barron and M. L. Klein, Proc. Phys. Soc. **85**, 523 (1965).
[55] P. M. Marcus and S. L. Qiu, J. Phys.: Condens. Matter **21**, 115401 (2009).
[56] M. W. Guinan and D. N. Beshers, J. Phys. Chem. Solids **29**, 541 (1968).
[57] S. Klotz and M. Braden, Phys. Rev. Lett. **85**, 3209 (2000).
[58] A. K. Singh, H. K. Mao, J. Shu, and R. J. Hemley, Phys. Rev. Lett. **80**, 2157 (1998).
[59] P. Söderlind, J. A. Moriarty, and J. M. Wills, Phys. Rev. B **53**, 14063 (1996).
[60] A. Landa, J. Klepeis, P. Söderlind, I. Naumov, O. Velikokhatnyi, L. Vitos, and A. Ruban, J. Phys. Chem. Solids **67**, 2056 (2006).
[61] L. Koci, Y. Ma, A. R. Oganov, P. Souvatzis, and R. Ahuja, Phys. Rev. B **77**, 214101 (2008).

[62] O. M. Krasilnikov, Y. K. Vekilov, I. Y. Mosyagin, E. I. Isaev, and N. G. Bondarenko, J. Phys.: Condens. Matter **24**, 195402 (2012).
[63] G. Grimvall, Thermophysical Properties of Materials – Enlarged and Revised Edition (North-Holland, Amsterdam, 1999).
[64] H. Hasegawa, M. W. Finnis, and D. G. Pettifor, J. Phys. F, Met. Phys. **15**, 19 (1985).
[65] E. I. Isaev, S. I. Simak, A. S. Mikhaylushkin, Y. K. Vekilov, E. Y. Zarechnaya, L. Dubrovinsky, N. Dubrovinskaia, M. Merlini, M. Hanfland, and I. A. Abrikosov, Phys. Rev. B **83**, 132106 (2011).
[66] P. Steneteg, O. Hellman, O. Y. Vekilova, N. Shulumba, F. Tasnadi, and I. A. Abrikosov, Phys. Rev. B **87**, 094114 (2013).
[67] O. Gülseren and R. E. Cohen, Phys. Rev. B **65**, 064103 (2002).
[68] L. Vočadlo, Earth Planet. Sci. Lett. **254**, 227 (2007).
[69] T. Gebhardt, D. Music, M. Ekholm, I. A. Abrikosov, J. von Appen, R. Dronskowski, D. Wagner, J. Mayer, and J. M. Schneider, Acta Mater. **59**, 1493 (2011).
[70] B. Alling, T. Marten, and I. A. Abrikosov, Nature Mater. **9**, 283 (2010).
[71] P. Steneteg, B. Alling, and I. A. Abrikosov, Phys. Rev. B **85**, 144404 (2012).
[72] J. M. Wills and W. A. Harrison, Phys. Rev. B **28**, 4363 (1983).
[73] C. Kittel, Introduction to Solid State Physics, fifth ed. (Wiley, New York, 1976).
[74] M. Nastar and F. Willaime, Phys. Rev. B **51**, 6896 (1995).
[75] T. Y. Zhang, W. Y. Chu, and C. M. Hsiao, Met. Trans. A **16A**, 1649 (1985).
[76] A. F. Bialon, T. Hammerschmidt, and R. Drautz, Phys. Rev. B **87**, 104109 (2013).
[77] P. Soven, Phys. Rev. **156**, 809 (1967).
[78] B. L. Györffy, Phys. Rev. B **5**, 2382 (1972).
[79] J. M. Sanchez, F. Ducastelle, and D. Gratias, Physica A **128**, 334 (1984).
[80] A. Zunger, S. H. Wei, L. G. Ferreira, and J. E. Bernard, Phys. Rev. Lett. **65**, 353 (1990).
[81] L. Vitos, I. A. Abrikosov, and B. Johansson, Phys. Rev. Lett. **87**, 156401 (2001).
[82] A. van de Walle, Nature Mater. **7**, 455 (2008).
[83] J. von Pezold, A. Dick, M. Friak, and J. Neugebauer, Phys. Rev. B **81**, 094203 (2010).
[84] H. Zhang, B. Johansson, and L. Vitos, Phys. Rev. B **79**, 224201 (2009).
[85] B. Magyari-Köpe, G. Grimvall, and L. Vitos, Phys. Rev. B **66**, 064210 (2002).
[86] Q. Williams, R. Jeanloz, J. D. Bass, B. Svendesen, and T. J. Ahrens, Science **236**, 181–182 (1987).
[87] A. P. Jephcoat and S. P. Besedin, Philos. Trans. R. Soc. Lond. A **354**, 1333 (1996).
[88] R. Boehler, Nature **363**, 534 (1993).
[89] G. Shen, H. Mao, R. J. Hemley, T. S. Duffy, and M. L. Rivers, Geophys. Res. Lett. **25**, 373–376 (1998).
[90] Y. Ma, G. Somayazulu, G. Shen, H. K. Mao, J. Shu, and R. J. Hemley, Phys. Earth Planet. Inter. **143-144**, 455 (2004).
[91] J. M. Jackson, W. Sturhahn, M. Lerche, J. Zhao, T. S. Toellner, E. E. Alp, S. V. Sinogeikin, J. D. Bass, C. A. Murphy, and J. K. Wicks, Earth Planet. Sci. Lett. **362**, 143 (2013).
[92] S. Anzellini, A. Dewaele, M. Mezouar, P. Loubeyre, and G. Morard, Science **340**, 464 (2013).
[93] J. M. Brown and R. G. McQueen, J. Geophys. Res. **91**, 7485–7494 (1986).
[94] J. H. Nguyen and N. C. Holmes, Nature **427**, 339–342 (2004).
[95] C. S. Yoo, N. C. Holmes, M. Ross, D. J. Webb, and C. Pike, Phys. Rev. Lett. **70**, 3931–3934 (1993).
[96] A. Laio, S. Bernard, G. L. Chiarotti, S. Scandolo, and E. Tosatti, Science **287**, 1027 (2000).
[97] A. B. Belonoshko, R. Ahuja, and B. Johansson, Phys. Rev. Lett. **84**, 3638 (2000).
[98] D. Alfè, M. J. Gillan, and G. D. Price, Nature **401**, 462–464 (1999).
[99] D. Alfè, G. D. Price, and M. J. Gillan, Phys. Rev. B **64**, 045123 (2001).
[100] D. Alfè, G. D. Price, and M. J. Gillan, Phys. Rev. B **65**, 165118 (2002).
[101] D. Alfè, G. D. Price, and M. J. Gillan, J. Chem. Phys. **116**, 6170 (2002).
[102] D. Alfè, Phys. Rev. B **79**, 060101(R) (2009).
[103] F. Körmann, A. Breidi, S. L. Dudarev, N. Dupin, G. Ghosh, T. Hickel, P. Korzhavyi, J. Munoz, and I. Ohnuma, Phys. Status Solidi B **251**, 53–80 (2014), this issue.
[104] V. Iota, J. H. P. Klepeis, C. S. Yoo, J. Lang, D. Haskel, and G. Srajer, Appl. Phys. Lett. **90**, 042505 (2007).
[105] R. Torchio, Y. O. Kvashnin, S. Pascarelli, O. Mathon, C. Marini, L. Genovese, P. Bruno, G. Garbarino, A. Dewaele, F. Occelli, and P. Loubeyre, Phys. Rev. Lett. **107**, 237202 (2011).
[106] A. I. Liechtenstein, M. I. Katsnelson, and V. A. Gubanov, J. Magn. Magn. Mater. **67**, 65 (1987).
[107] W. Olovsson and I. A. Abrikosov, J. Appl. Phys. **97**, 10A317 (2005).
[108] A. V. Ruban, M. I. Katsnelson, W. Olovsson, S. I. Simak, and I. A. Abrikosov, Phys. Rev. B **71**, 054402 (2005).
[109] L. Dubrovinsky, N. Dubrovinskaia, I. A. Abrikosov, M. Vennström, F. Westman, S. Carlson, M. van Schilfgaarde, and B. Johansson, Phys. Rev. Lett. **86**, 4851 (2001).
[110] R. M. Martin, Electronic Structure. Basic Theory and Practical Methods (Cambridge University Press, Cambridge, 2004).
[111] Y. S. Mohammed, Y. Yan, H. Wang, K. Li, and X. Du, J. Magn. Magn. Mater. **322**, 653 (2010).
[112] F. Körmann, A. Dick, T. Hickel, and J. Neugebauer, Phys. Rev. B **79**, 184406 (2009).
[113] X. Sha and R. E. Cohen, J. Phys.: Condens. Matter **22**, 372201 (2010).
[114] J. Xie, S. P. Chen, H. V. Brand, and R. L. Rabie, J. Phys.: Condens. Matter **12**, 8953 (2000).
[115] V. P. Antropov, M. I. Katsnelson, M. van Schilfgaarde, and B. N. Harmon, Phys. Rev. Lett. **75**, 729 (1995).
[116] I. A. Abrikosov, A. E. Kissavos, F. Liot, B. Alling, S. I. Simak, O. E. Peil, and A. V. Ruban, Phys. Rev. B **76**, 014434 (2007).
[117] M. van Schilfgaarde, I. A. Abrikosov, and B. Johansson, Nature **400**, 46 (1999).
[118] M. Ekholm, H. Zapolsky, A. V. Ruban, I. Vernyhora, D. Ledue, and I. A. Abrikosov, Phys. Rev. Lett. **105**, 167208 (2010).
[119] G. Steinle-Neunmann, L. Stixrude, and R. E. Cohen, Phys. Rev. B **60**, 791 (1999).
[120] G. Steinle-Neunmann, L. Stixrude, and R. E. Cohen, J. Phys.: Condens. Matter **16**, S1109 (2004).

[121] R. Lizárraga, L. Nordström, O. Eriksson, and J. Wills, Phys. Rev. B **78**, 064410 (2008).
[122] A. B. Papandrew, M. S. Lucas, R. Stevens, I. Halevy, B. Fultz, M. Y. Hu, P. Chow, R. E. Cohen, and M. Somayazulu, Phys. Rev. Lett. **97**, 087202 (2006).
[123] A. Georges, G. Kotliar, W. Krauth, and M. J. Rozenberg, Rev. Mod. Phys. **68**, 13 (1996).
[124] G. Kotliar, S. Y. Savrasov, K. Haule, V. S. Oudovenko, O. Parcollet, and C. A. Marianetti, Rev. Mod. Phys. **78**, 865 (2006).
[125] K. Glazyrin, L. V. Pourovskii, L. Dubrovinsky, O. Narygina, C. McCammon, B. Hewener, V. Schünemann, J. Wolny, K. Muffler, A. I. Chumakov, W. Crichton, M. Hanfland, V. B. Prakapenka, F. Tasnádi, M. Ekholm, M. Aichhorn, V. Vildosola, A. V. Ruban, M. I. Katsnelson, and I. A. Abrikosov, Phys. Rev. Lett. **110**, 117206 (2013).
[126] R. Car and M. Parrinello, Phys. Rev. Lett. **55**, 2471 (1985).
[127] L. Vočadlo, D. Alfè, M. J. Gillan, I. G. Wood, J. P. Brodholt, and G. D. Price, Nature **76**, 536 (2003).
[128] L. Kaufman, in: Phase Stability in Metals and Alloys, edited by P. S. Rudman, I. Stringer, and R. I. Jaffee (McGraw-Hill, New York, 1967), p. 125.
[129] L. Kaufman and H. Bernstein, Computer Calculations of Phase Diagrams (Academic Press, New York, 1970).
[130] A. F. Guillermet, V. Ozoliņš, G. Grimvall, and M. Körling, Phys. Rev. B **51**, 10364 (1995).
[131] K. Persson, M. Ekman, and G. Grimvall, Phys. Rev. B **60**, 9999 (1999).
[132] P. E. A. Turchi, I. A. Abrikosov, B. Burton, S. G. Fries, G. Grimvall, L. Kaufman, P. A. Korzhavyi, V. R. Manga, M. Ohno, A. Pisch, A. Scott, and W. Zhang, Calphad **31**, 4 (2007).
[133] P. Souvatzis, O. Eriksson, M. I. Katsnelson, and S. P. Rudin, Phys. Rev. Lett. **100**, 095901 (2008).
[134] C. Asker, A. B. Belonoshko, A. S. Mikhaylushkin, and I. A. Abrikosov, Phys. Rev. B **77**, 220102(R) (2008).
[135] V. Ozoliņš, Phys. Rev. Lett. **102**, 065702 (2009).
[136] M. J. Gillan, D. Alfè, J. Brodholt, L. Vočadlo, and G. D. Price, Rep. Prog. Phys. **69**, 2365–2441 (2006).
[137] O. Hellman, I. A. Abrikosov, and S. I. Simak, Phys. Rev. B **84**, 180301(R) (2011).
[138] O. Hellman, P. Steneteg, I. A. Abrikosov, and S. I. Simak, Phys. Rev. B **87**, 104111 (2013).
[139] http://web.access.rwth-aachen.de/MICRESS/.
[140] http://www.openphase.de/.

